Self-Consistent Dynamics of Impurities in Magnetically Confined Plasmas: Turbulence Intermittency and Nondiffusive Transport

S. Futatani,[1] D. del-Castillo-Negrete,[2] X. Garbet,[3] S. Benkadda,[4] and N. Dubuit[4]

[1]*ITER Organization, Route de Vinon sur Verdon, 13115 Saint Paul les Durance, France*
[2]*Oak Ridge National Laboratory, Oak Ridge, Tennessee 37831-8071, USA*
[3]*CEA, IRFM, F-13108 Saint Paul-Lez-Durance, France*
[4]*International Institute for Fusion Science/PIIM, Aix Marseille Université-CNRS Campus Saint Jerome, Case 321, 13397 Marseille Cedex 20, France*

(Received 30 March 2012; published 2 November 2012)

Self-consistent turbulent transport of high-concentration impurities in magnetically confined fusion plasmas is studied using a three-dimensional nonlinear fluid global turbulence model which includes ion-temperature gradient and trapped electron mode instabilities. It is shown that the impurity concentration can have a dramatic feedback in the turbulence and, as a result, it can significantly change the transport properties of the plasma. High concentration impurities can trigger strong intermittency that manifests in non-Gaussian heavy tails of the probability density functions of the $\mathbf{E} \times \mathbf{B}$ fluctuations and of the ion-temperature flux fluctuations. At the heart of this self-consistent coupling is the existence of inward propagating ion-temperature fronts with a sharp gradient at the leading edge that give rise to instabilities and avalanchelike bursty transport. Numerical evidence of time nonlocality (i.e., history dependence) in the delayed response of the flux to the gradient is presented.

DOI: 10.1103/PhysRevLett.109.185005 PACS numbers: 52.25.Fi, 52.35.Ra, 52.55.Fa

The performance of magnetically confined fusion plasmas in general, and of ITER in particular, can be critically affected by impurities. The accumulation of impurities in the core can lead to radiation losses and fuel dilution detrimental to energy confinement. Thus, a key issue of the magnetically confined plasma fusion program is the understanding of impurity transport. An often used approximation is to treat the impurity as a passive scalar ignoring the back reaction on the turbulence. Although this approximation is reasonable and has yielded valuable insights when the impurity concentration is low, e.g., Refs. [1], it might break down when the impurity concentration is high like in experiments involving plasma radiative cooling [2]. Beyond the aforementioned relevance to fusion plasmas, the study of transport of active scalars, i.e., scalars that modify the underlying advection flow, is a problem of broad theoretical and practical interest. Well-known, important examples include transport of temperature in turbulent convection [3], the magnetic dynamo problem [4], potential vorticity mixing in geophysical flows [5], and self-consistent chaotic transport in fluids and plasmas [6] among others. Although the physics mechanisms of the self-consistent coupling is different in these problems, at a fundamental level, the descriptions of these active scalar transport problems share important similarities.

Here we focus on the self-consistent coupling between the dynamics of the impurity density (treated as an active scalar) and the $\mathbf{E} \times \mathbf{B}$ turbulence in a magnetically confined fusion plasma. The novel results presented pertain to both the $\mathbf{E} \times \mathbf{B}$ turbulence and the transport of the impurity itself. Regarding the $\mathbf{E} \times \mathbf{B}$ turbulence, we show that a high concentration of impurities leads to a qualitative transition from a stationary state, characterized by Gaussian probability density functions (PDFs) of the fluctuations, to strongly intermittent states, characterized by non-Gaussian PDFs. This transition also manifests in the ion thermal flux leading to bursty transport. The culprit of this transition is the self-consistent coupling between the impurity and the flow that leads to the creation of strong gradients in the ion-temperature profile that exhibit an inward front propagation. We show that this transition is accompanied by a transition in the impurity density evolution from a diffusive transport regime to a nondiffusive transport regime characterized by non-Fickian flux-gradient relations. Contrary to what would be expected within the diffusive (Fickean) description, the time cross-correlation function between the impurity flux, Γ_z, and the impurity density gradient, ∇n_z, exhibits a shift in the maximum due to a delay in the response of the flux to the gradient when the impurity concentration is high. An effective nonlocal in time (history dependent) model relating the flux and the gradient is proposed to describe the system in the spatiotemporal transport scale. A Laplace transform method is proposed to obtain from the numerical data the functional form of the nonlocal operator (memory kernel) relating Γ_z and ∇n_z.

Our study is based on the three-dimensional nonlinear fluid global turbulence model originally proposed in Refs. [7], which includes ion-temperature gradient (ITG) and trapped electron (TEM) instabilities. The model evolves the trapped electron, ion, and impurity pressures, the trapped

electron and impurity densities, the ion and impurity parallel velocities, and the vorticity. Passing electrons are assumed to be adiabatic, and the parallel velocity of the trapped electrons is assumed zero. The fraction of trapped (passing) electrons is $f_t = 2/\pi(2r/R)^{1/2}$ ($f_c = 1 - f_t$) where R is the plasma major radius. The ion density n_i is obtained from ambipolarity in terms of the vorticity, Ω according to $\Omega = f_c n_{e,eq} \frac{\phi - \phi_{eq}}{T_{e,eq}} - (n_{i,eq} + A n_{z,eq})\nabla^2\phi$, where the subindex "$eq$" denotes flux average, and ϕ is the electrostatic potential. Further details of the model can be found in Refs. [7]. The parameter values used in the simulations are the adiabatic compression index, $\gamma = 5/3$, normalized Larmor radius, $\rho_* = 6 \times 10^{-3}$, ratio of the minor to major radius, $a/R = 1/3$, sound speed, $c_s = 7.58 \times 10^5$ [m/s], q profile, $q_{r/a=0} = 0.8$, $q_{r/a=1.0} = 3.3$. The calculations are performed at fixed flux. The main impurity used is nickel which is introduced during the steady state turbulence as an instantaneous perturbation. We present a comparative study of low and high impurity concentrations. In the low (high) concentration case, the concentration of the nickel pulse at the time of injection is 0.03% (0.3%) of the average impurity content if distributed as the electron density. The corresponding *local* (at the point of injection) impurity density concentrations are 48% and 4.8% for the high-concentration and the low-concentration cases respectively. Note that, although these numbers are high, the pulse is very localized and thus the global average impurity concentrations are much smaller, 0.3% and 0.03%, as mentioned before. A nickel impurity concentration of order 0.3% is compatible with ignited plasmas for $\langle T_e \rangle > 14$ keV [8].

As a simplified model of impurity injection, we assume an instantaneous pulse initial condition. As shown in Fig. 3(b) (black solid line), the pulse shape is a narrow, radially symmetric, toroidal shell centered at $r/a = 0.8$. The TRB code has a "buffer zone" of the order $r/a \sim 0.1$ and thus $r/a = 0.8$ in the simulations corresponds to $r/a \sim 0.9$ in the physical domain, i.e., the plasma edge. A fully realistic model of the precise way in which impurities are actually introduced in fusion plasma experiments is outside the scope of this work. However, to assess the degree to which the results depend on the pulse injection model, we have performed extensive numerical simulations for different initial conditions. Although the detailed account of these simulations will be published elsewhere, below we discuss the lack of dependence of the main results on the specific details and/or peculiarities of the adopted impurity injection model.

The first evidence of the dynamic coupling between the impurity injection and the turbulence is reported in Fig. 1. For low concentration of a nickel impurity, the $\mathbf{E} \times \mathbf{B}$ velocity fluctuations exhibit a Gaussian distribution. However, for high concentration, the self-consistent coupling between the impurity dynamics and the turbulence gives rise to strongly intermittent velocity fluctuations which result in a non-Gaussian tail of the corresponding PDF. The time

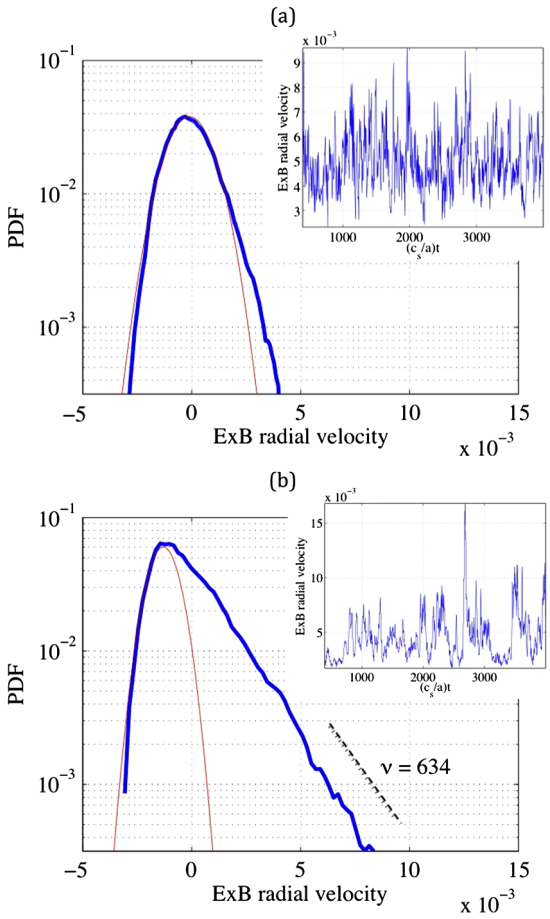

FIG. 1 (color online). Impurity-driven intermittency. The main panels show the PDF of $\mathbf{E} \times \mathbf{B}$ velocity fluctuations, $\widetilde{\mathbf{E} \times \mathbf{B}} = \mathbf{E} \times \mathbf{B} - \langle \mathbf{E} \times \mathbf{B} \rangle$ in blue with a Gaussian fit in red. The inserts show the time series at $r/a = 0.5$. The top (bottom) figure corresponds to low (high) nickel impurity concentration for which $\langle \mathbf{E} \times \mathbf{B} \rangle = 4.8 \times 10^{-3}$ ($\langle \mathbf{E} \times \mathbf{B} \rangle = 4.0 \times 10^{-3}$). The dashed line in (b) indicates an exponential decay, $\sim e^{-\nu x}$, with $\nu \sim 634$.

reported in all the figures has been nondimensionalized using the time scale c_s/a, and by definition, $t = 0$ corresponds to the time of the injection of the pulse. The fluctuations relax after $(c_s/a)t > 4000$ and eventually die out after $(c_s/a)t > 6000$. We have also performed extensive computations with other impurities including helium, nitrogen, argon, and krypton, and concluded that the level of intermittency increases with the charge number of the impurity.

Figure 2 shows the spatiotemporal evolution of the ion thermal flux. Throughout the Letter, the spatial dependence of the results are presented only as a function of r because they correspond to flux-average quantities. For a nickel impurity, the ion-temperature fluctuations become stronger (by a factor of 2) and intermittent. In particular, the PDF of ion-temperature fluctuations (i.e., with the mean subtracted) transitions from a near Gaussian profile in the low nickel impurity concentration case, to a skewed, non-Gaussian

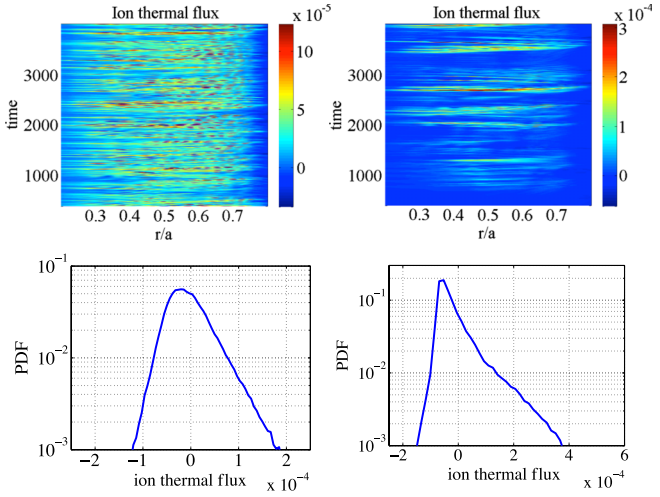

FIG. 2 (color online). The effect of impurity concentration on the ion-temperature flux. The top two panels show the spatiotemporal evolution of the ion-temperature flux. The bottom panels show the corresponding PDFs of the fluctuations of the ion-temperature flux at $r/a = 0.5$. The left column corresponds to low nickel impurity concentration, and the right column corresponds to high nickel impurity concentration.

PDF with heavy tails in the high nickel impurity concentration case. In the low (high) impurity concentration case, the mean ion temperature is 6.23×10^{-5} (5.72×10^{-5}). Figure 3 shows the radial temperature profiles at successive times following the introduction of the impurity. In the low concentration case, the interaction is negligible and the temperature profile remains practically unchanged. In the high concentration case, the impurity acts as an active scalar and the temperature profiles are significantly modified. In particular, an inward propagating temperature front with a sharp gradient at the leading edge is observed. This front, in turn, triggers ion-temperature instabilities responsible for the intermittency observed in Fig. 1, and the avalanchelike bursty transport observed in Fig. 4. The peaking of the density profile at $r/a = 0.8$ is not evident in Fig. 4 because in this figure we eliminated the transient phase, $0 < t < 500$, for visualization purposes. Similar behavior is observed in reduced models of plasma turbulence [9]. The effect of the concentration level in the impurity transport is shown in Fig. 4 which shows the spatiotemporal evolution of the impurity density for low (a) and high (b) concentration. "Bursty" transport is observed in the high-concentration case, caused by the impurity-driven intermittency in the $\mathbf{E} \times \mathbf{B}$ turbulence shown in Fig. 1.

To address the dependence of the results on the impurity injection model, we have performed extensive numerical simulations changing the shape, width, and amplitude of the initial impurity profile. In particular, as a more realistic model of the way impurities might enter the plasma (e.g., laser blow-off experiments) we have considered asymmetric initial profiles with a broader tail towards the edge to account for the spatial spreading of the impurity as it penetrates the plasma [see dashed line in Fig. 3(b)]. We have observed the same phenomenology for these asymmetric profiles and concluded that what matters is not the spatial localization of the impurity, but the presence of a sharp gradient in the leading edge (i.e., towards the core) of the impurity profile. Another issue of interest is the description of the impurity perturbation as an instantaneous pulse initial condition versus a time dependent source. Numerical simulations indicate that the latter option typically enhances the observed intermittency as the strong density gradient (responsible for the triggering the instabilities) acts longer. The exception to this scenario is when the time scale of the impurity source is slower than the growth rate of the instabilities triggering the intermittent plasma response. In this case, the plasma exhibits an adiabatic response and the impurity is transported as a passive scalar.

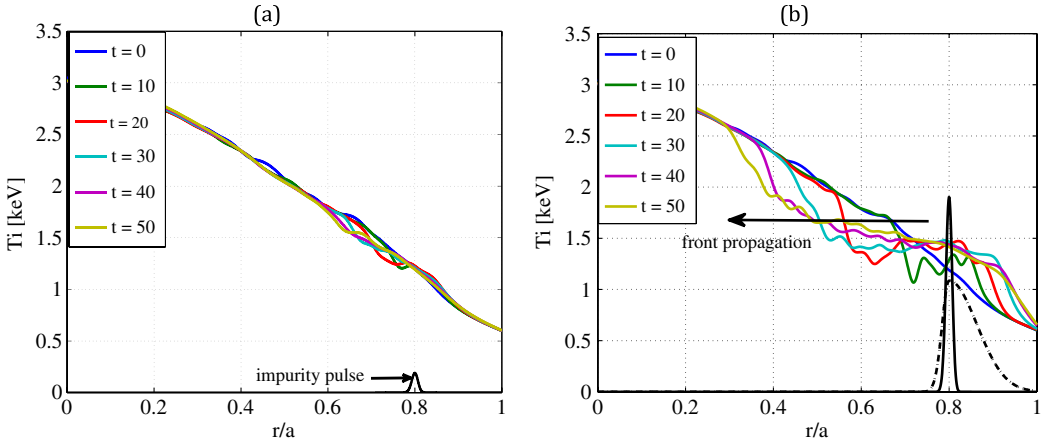

FIG. 3 (color online). Inward front propagation of ion-temperature perturbations due to self-consistent impurity driven turbulence for low (a), and high (b), impurity concentration. The scale of the impurity density pulse is $\times 10^{19}$ m^{-3}. The solid (dashed) black curve on (b) corresponds to a localized symmetric (spread asymmetric) initial condition. In panel (b), the different curves from left to right correspond to $t = 50$, 40, 30, 20, 10 and 0.

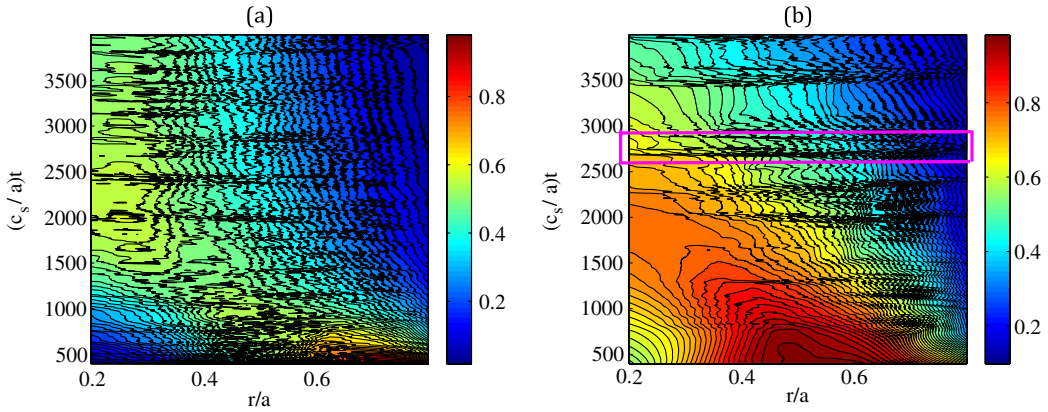

FIG. 4 (color online). Spatiotemporal evolution of the normalized impurity density pulse for low, panel (a), and high, panel (b), impurity concentrations. The small rectangle in (b), isolates a single avalanchelike event leading to a "bursty" transport of the impurity.

To conclude, we present numerical evidence of nonlocal transport of impurities in the high-concentration case. Following Ref. [10], by nonlocal transport we mean that the flux, Γ_z, at a given point in space, r, at a given time, t, depends on the gradient, ∇n_z, over the whole domain (in the case of spatial nonlocality) and over the time history (in the case of temporal nonlocality) of ∇n_z, i.e., $\Gamma_z(r,t) = -D\int d\rho \int_0^t d\tau \mathcal{L}(r,t;\rho,\tau)\nabla n_z(\rho,\tau)$, where the kernel $\mathcal{L}(r,t;\rho,\tau)$ determines the properties of the spatiotemporal nonlocal response. Our working hypothesis is that, in the high impurity concentration case, there is memory in the flux-gradient relation which we model as $\Gamma_z(r,t) = -D\int_0^t d\tau \mathcal{K}(t-\tau)\nabla n_z(r,\tau)$, where Γ_z is the effective impurity density flux in the spatiotemporal transport scale. To get the kernel function, $\mathcal{K}$, we perform a Laplace transform on the flux and obtain $\tilde{\mathcal{K}}(s) = -\tilde{\Gamma}/(D\tilde{\nabla} n_z)$, where $\tilde{f}(s) = \int_0^\infty e^{-s\tau} f(\tau) d\tau$. An inversion of the Laplace transform is then performed to get $\mathcal{K}(\tau)$. The result of this procedure, for a fixed $(r/a = 0.5)$ radius, is reported in Fig. 5(a) which shows $\mathcal{K}(\tau)$ obtained from the density data in Fig. 4, and the flux data (not shown). It is observed that the decay of $\mathcal{K}(\tau)$ can be fitted by the normalized exponential function $\mathcal{K}(\tau) = \lambda e^{-\lambda\tau}$. As indicated in Fig. 5(a), in the low (high) impurity concentration case, $\lambda_l = 3.5 \times 10^{-3}$ ($\lambda_h = 0.9 \times 10^{-3}$).

The memory, $\langle\tau\rangle = \int_0^\infty \tau\mathcal{K}(\tau)d\tau = 1/\lambda$, in the high impurity concentration case, $\langle\tau\rangle_h \sim 1100$, is longer than the memory in the low impurity concentration case, $\langle\tau\rangle_l \sim 285$. Most importantly, $\langle\tau\rangle_h$ is much longer than the time scale of the turbulent fluctuations (see Fig. 1), and it encompasses several bursting transport events both in the ion thermal fluctuations (see Fig. 2) and in the impurity density evolution (see Fig. 4). This indicates that the memory is a property of the macroscopic time scale. According to Fig. 3, $\langle\tau\rangle_h$ is also of the same order of magnitude as the inward front propagation time scale. When the Fourier-Fick's prescription applies, the cross-correlation function, $C(\tau) = \int dr \int dt \Gamma_z(r,t+\tau)\nabla n_z(r,t)$, peaks at $\tau_{\max} = 0$. Accordingly, a shift of the extremum of

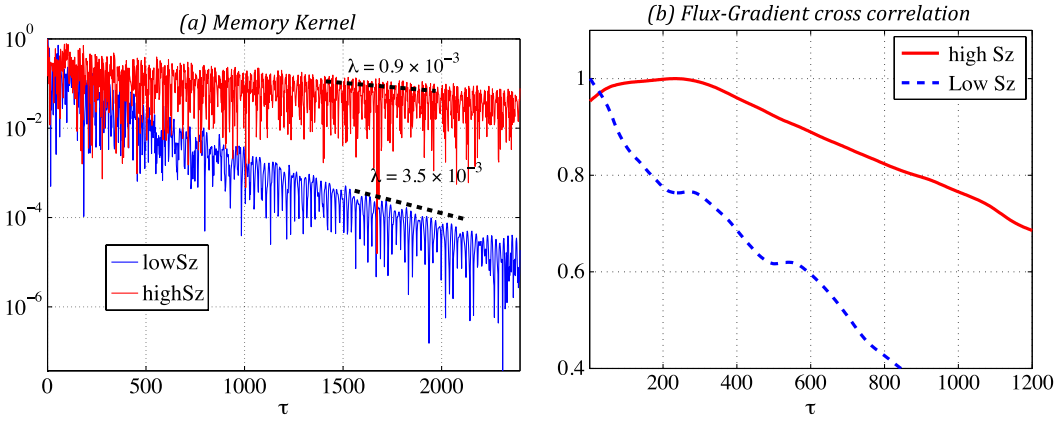

FIG. 5 (color online). Transition to nonlocal (in time) turbulent transport due to high-concentration impurities. (a) Memory kernel function, $\mathcal{T}(\tau)$, at $r/a = 0.5$. The slowly (rapidly) decaying function corresponds to the high (low) impurity concentration case. (b) Flux-gradient time-cross correlation function. The dashed (solid) line corresponds to low (high) impurity concentration. In panel (a), the top (bottom) curve corresponds to high (low) impurity concentration.

$C(\tau)$ to $\tau_{\max} \neq 0$, resulting from a delay in the response of the flux to a change in the gradient, is indicative of nondiffusive transport. As Fig. 5(b) shows, this is precisely what happens in the high impurity concentration case, where $\tau_{\max} \sim 250$. To establish a connection between the memory and $\tau_{\max}$ in an analytically tractable setting, consider a density gradient of the form $\nabla n_z \sim e^{-\mu t}$ providing a simple model for the relaxation of the impurity density following an avalanchelike event, like the one indicated in the rectangle in Fig. 4(b). In this case, $\tau_{\max} = \ln[2\lambda/(\lambda + \mu)]/(\lambda - \mu)$. Assuming a time scale of the event of the order $\sim$150, we chose $\mu \sim 1/150$, and for $\lambda_h = 0.9 \times 10^{-3}$ [see Fig. 5(a)], conclude $\tau_{\max} \sim 250$, a value consistent with the shift in $C(\tau)$ observed in Fig. 5(b).

S. F. acknowledges ITER-Monaco Postdoctoral Fellowships support. D. d-C-N. was supported by the US Department of Energy at Oak Ridge National Laboratory, managed by UT-Battelle, LLC, for the U.S. Department of Energy under Contract No. DE-AC05-00OR22725. D. d-C-N. thanks the International Institute for Fusion Sciences for hospitality during the elaboration of part of this work. This work was supported by the European Community, within the framework of the European Fusion Development Agreement. The views and opinions expressed herein do not necessarily reflect those of the European Commission or those of the ITER Organization.

[1] M. Priego, O. E. Garcia, V. Naulin, and J. Juul Rasmussen, Phys. Plasmas **12**, 062312 (2005); C. Estrada-Mila, J. Candy, and R. E. Waltz, Phys. Plasmas **12**, 022305 (2005); C. Angioni and A. G. Peeters, Phys. Rev. Lett. **96**, 095003 (2006); M. E. Puiatti, M. Valisa, C. Angioni, L. Garzotti, P. Mantica, M. Mattioli, L. Carraro, I. Coffey, C. Sozzi, and JET-EFDA contributors, Phys. Plasmas **13**, 042501 (2006); S. Futatani, S. Benkadda, and D. del-Castillo-Negrete, Phys. Plasmas **16**, 042506 (2009); S. Futatani, X. Garbet, S. Benkadda, and N. Dubuit, Phys. Rev. Lett. **104**, 015003 (2010); T. Fulop and H. Norman, Phys. Plasmas **16**, 032306 (2009); H. Nordman, A. Skyman, P. Strand, C. Giroud, F. Jenko, F. Merz, V. Naulin, and T. Tala, Plasma Phys. Controlled Fusion **53**, 105005 (2011).

[2] P. Mantica and F. Ryter, C.R. Physique **7**, 634 (2006); P. Mantica *et al.*, Report No. EX/P1-04, IAEA, 2010.

[3] E. D. Siggia, Annu. Rev. Fluid Mech. **26**, 137 (1994).

[4] F. H. Busse, Annu. Rev. Fluid Mech. **32**, 383 (2000).

[5] M. E. McIntyre and T. N. Palm, Nature (London) **305**, 593 (1983).

[6] D. del-Castillo-Negrete, Chaos **10**, 75 (2000).

[7] X. Garbet and R. E. Waltz, Phys. Plasmas **3**, 1898 (1996); N. Dubuit, X. Garbet, T. Parisot, R. Guirlet, and C. Bourdelle, Phys. Plasmas **14**, 042301 (2007).

[8] R. V. Jensen *et al.*, Nucl. Sci. Eng. **65**, 282 (1978).

[9] T. S. Hahm, P. H. Diamond, Z. Lin, K. Itoh, and S.-I. Itoh, Plasma Phys. Controlled Fusion **46**, A323 (2004).

[10] D. del-Castillo-Negrete, Phys. Plasmas **13**, 082308 (2006).